



37 the fire itself (e.g. Wotawa and Trainer, 2000; Forster et al., 2001). These forest  
38 fires are occasionally caused by human activity, but most (approximately 85%)  
39 are caused by lightning (Weber and Stocks, 1998). Episodically, organic car-  
40 bon (OC) emissions from boreal fires are the dominant source of regional  
41 levels of OC for the eastern and south-eastern United States, a region with one  
42 of the highest anthropogenic emission rates worldwide (Wotawa and Trainer,  
43 2000). Transport of forest fire plumes originating in Canada towards the  
44 United States is not uncommon (Skinner et al., 1999). Furthermore, the an-  
45 nual average area of burned forest has more than doubled since the 1970s  
46 (Skinner et al., 2002). By the first week of July 2002, fires in the Québec  
47 region had consumed some 162,000 ha of forest, twice as much as the annual  
48 average.

49 It is often due to large-scale subsidence that the aerosol from the forest  
50 fires is forced down to low altitudes, after it has been advected horizontally  
51 with the prevailing winds (Iziomon and Lohmann, 2003). If so, the smoke-  
52 laden air from higher altitudes is likely to intersect the atmospheric bound-  
53 ary-layer (ABL), and thereafter a type of 'fumigation' process distributes the  
54 gases and aerosols within the turbulent ABL. The haze event in Baltimore  
55 from July 6 to 8, 2002, resulted in the strong impact of combustion products  
56 such as black carbon, organic carbon and PM<sub>2.5</sub> (particulate matter with an  
57 aerodynamic diameter  $\leq 2.5 \mu\text{m}$ ) on a region remote from the fire origin.  
58 Events such as this emphasise the importance of improving our under-  
59 standing of gas and aerosol transport into the ABL from aloft, particularly  
60 because smoke aerosols can affect health, surface temperature (Robock, 1988  
61 a, b) and regional climate (Menon et al., 2002).

62 There is a long observational history of studies that examine ABL struc-  
63 ture and time evolution. Different techniques and a variety of instrumenta-  
64 tion probing the ABL, have been employed in the field (see references in Stull  
65 (1988) and Garratt (1992), and more recently e.g. Angevine et al. (1998a),  
66 Menut et al. (1999) and Yi et al. (2001)). Laboratory experiments have helped  
67 to further our understanding on distinct processes (e.g. Deardorff et al., 1980;  
68 Fedorovich and Thäter, 2002), while large-eddy simulation has also been  
69 used to study specific ABL processes in great detail (e.g. Wyngaard and  
70 Brost, 1984; Sullivan et al., 1998; Albertson and Parlange, 1999).

71 Here we present results from an experimental study in Baltimore, MD in the  
72 U.S.A. where smoke from forest fires in Québec was entrained into the ABL  
73 from aloft. The goal of this particular investigation is to provide a detailed  
74 description of the boundary-layer structure during the haze event and to link  
75 ABL processes with meteorological conditions and aerosol concentration at  
76 ground level. A comparison is made between the relatively clean atmosphere  
77 on July 6, the heavily polluted conditions on July 7, and the aftermath on July  
78 8, which was characterised by a slow cleansing process. Most of the obser-  
79 vations presented in this paper are from the Johns Hopkins University (JHU)



80 lidar supported by ground-based point sensors to characterise aerosol size and  
81 composition, as well as data from a micrometeorological station.

## 2. Experiment

83 Particulate matter (PM) Supersites is an ambient monitoring research pro-  
84 gram, funded by the U.S. Environmental Protection Agency (EPA). The  
85 program addresses the scientific uncertainties associated with fine particulate  
86 matter. The programs of the eight PM Supersites, operated during 1999–2003  
87 around the United States, focus on fine particulate characterisation, methods'  
88 testing, and support to health effects and exposure studies. Observations taken  
89 in the context of the Supersite project in Baltimore are intended to provide an  
90 extended, highly time, size, and compositionally resolved dataset, including an  
91 indicator of cardiopulmonary response in support of testing hypotheses  
92 relating to source attribution and health effects of PM.

93 Here we report on observations made at the Ponca St. sampling site in  
94 downtown Baltimore (39° 17' 20" N, 76° 33' 16" W, elevation approximately  
95 40 m above sea level), during a haze event caused by forest fires in Québec,  
96 Canada, from July 6 to 8, 2002. To characterise atmospheric boundary-layer  
97 dynamics, meteorological conditions and atmospheric aerosols, data obtained  
98 with the following instruments are analysed. The JHU elastic backscatter lidar  
99 system (see Pahlow (2002) for a full system description), a micrometeoro-  
100 logical tower, an integrating nephelometer operating at 530 nm (Radiance  
101 Research Model M-903), a tapered element oscillating microbalance (TEOM)  
102 and a semi-continuous elemental and organic carbon (EC/OC) monitor, the  
103 latter three all mounted at a height  $z = 3.5$  m.

104 The lidar system was operated at 1064 nm in upward pointing mode at  
105 ground level, with a time resolution of 5 s and a range resolution of 3.75 m.  
106 The micrometeorological tower was instrumented with a pyranometer  
107 ( $z = 11.0$  m), a wind vane ( $z = 10.4$  m), two cup anemometers ( $z = 5.8$  and  
108 10.4 m), a hygrometer ( $z = 4.9$  m), a rain gauge ( $z = 3.0$  m) and a pressure  
109 sensor ( $z = 2.5$  m). Micrometeorological and nephelometer data were re-  
110 corded as 5-min averages. The TEOM provided fine particle mass concen-  
111 tration, integrated over 30-min intervals, and the elemental and organic  
112 carbon monitor gave data integrated over 1 h periods. Note that local  
113 standard time (LST) is used throughout this discussion, which corresponds to  
114 eastern daylight time (EDT) for the time period studied here.

## 3. Canadian Forest Fires: Causes and Consequences

116 Starting July 2, 2002, some 85 forest fires broke out in two regions south-east  
117 of James Bay, central Québec, 350–650 km north of the U.S. border. A

118 combination of prevailing drought conditions in eastern North America and  
119 lightning strikes initiated the fires. Strong winds enhanced fire intensity. The  
120 fires, some of them burning out of control, produced large amounts of  
121 smoke. The smoke was advected southward to the north-eastern U.S.A. and  
122 the Atlantic Ocean as a cyclone intensified over the Canadian Maritimes and  
123 reached parts of the mid-Atlantic region, including Maryland and the city of  
124 Baltimore, by July 6, 2002. The MODIS satellite image (Figure 1) from July  
125 7, 2002, outlines active forest fires and the pathway of the forest-fire smoke.  
126 High pressure subsidence forced the smoke to lower altitudes. Figure 2a  
127 shows the time series of atmospheric pressure recorded at the Baltimore PM  
128 Supersite during July 6–8, 2002. Northerly winds advected the smoke to  
129 Baltimore on July 6 (Figure 2b); weak winds elongated the residence time of  
130 smoke in the ABL (Figure 2c). The smoke signature can clearly be seen in the  
131 time series of solar radiation (SR) (Figure 2d). The maximum SR on cloud-

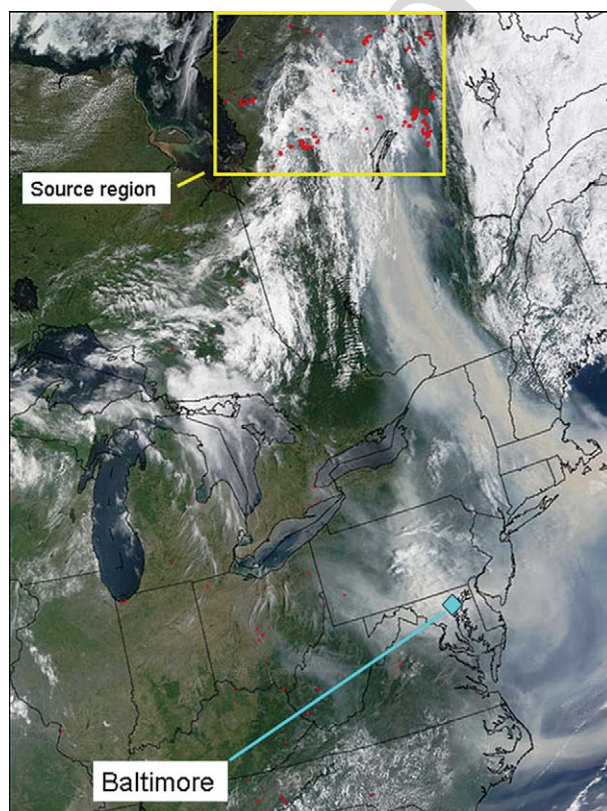


*Figure 1.* MODIS satellite image taken on July 7, 2002 at 1035 LST. The red dots represent active forest fires. The pathway of the smoke plume from Québec to the eastern United States can clearly be seen. MODIS satellite image courtesy of Land Rapid Response Team, NASA/GSFC, Greenbelt, MD, U.S.A.

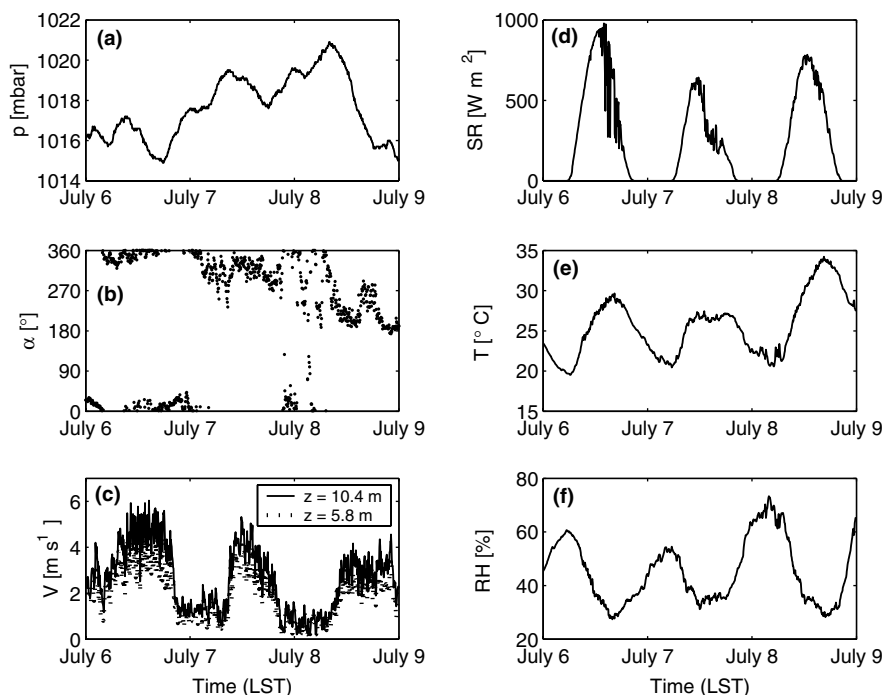


Figure 2. (a) Atmospheric pressure  $p$ , (b) wind direction  $\alpha$ , (c) horizontal wind speed  $V$  measured at two heights, (d) solar radiation, SR, (e) air temperature  $T$  and (f) relative humidity, RH at the Ponca St. field site in Baltimore during July 6–8, 2002. Tick marks along the abscissa axis denote midnight.

132 free July 7, the peak period of the haze event, is 34% lower than that on July  
 133 6, where clouds prevailed in the afternoon, and 18% lower than that on July  
 134 8, a day with little cloud cover. This, in turn, affects air temperature (Fig-  
 135 ure 2e), with a July 7 maximum that is 2.3 °C lower than the maximum on  
 136 July 6 and 6.8 °C lower than the maximum on July 8. The mean air tem-  
 137 perature on July 7 fell 2.8 °C below the monthly mean air temperature.  
 138 Relative humidity (RH) was low during the forest-fire peak event, about 10–  
 139 15% below typical July values (Figure 2f); in the early afternoon of July 8,  
 140 the atmospheric pressure fell. This indicated the approach of a cold front,  
 141 which, together with a shift in wind direction (Figure 2c), directed the smoke  
 142 eastward over the Atlantic, ending the haze event.

#### 4. Visibility and Aerosol Properties

144 To illustrate how the smoke aerosols influenced various parts of the east  
 145 coast of the U.S.A. in particular Baltimore and the vicinity, we present

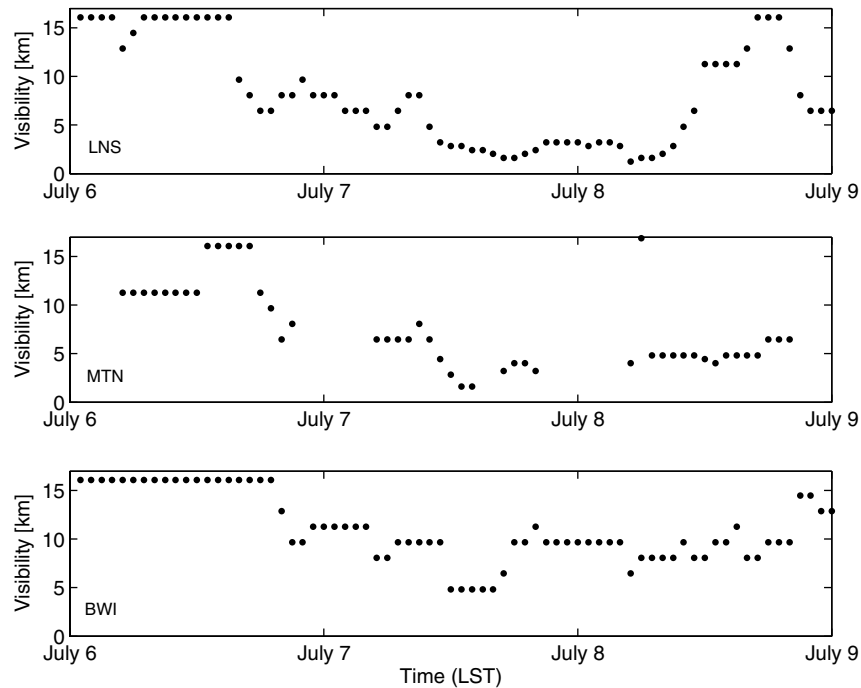


Figure 3. Visibility at three airports (top: LNS, middle: MTN and bottom: BWI) during July 6–8, 2002. The maximum visibility recorded at airports is 16 km. Tick marks along the abscissa axis denote midnight.

146 visibility measurements at airports in Figure 3. Lancaster airport [(LNS) 40°  
 147 7' 18" N, 76° 17' 45" W] is located 95 km north of Baltimore, Martin State  
 148 airport [(MTN) 39° 19' 32" N, 76° 24' 49" W] is 15 km east of Baltimore, and  
 149 Baltimore–Washington International airport [(BWI) 39° 10' 31" N, 76° 40'  
 150 6" W] is 15 km south of Baltimore. Figure 3 clearly shows that visibility is  
 151 decreased strongly by the forest-fire smoke, and that all three locations are  
 152 affected, starting in the evening of July 6. The impact of aerosols on visibility  
 153 over the 3-day period under consideration is strongest at LNS, with a min-  
 154 imum visibility of 1.2 km. At the other two locations the minimum is re-  
 155 corded as 1.6 km at MTN and 4.8 km at BWI, respectively. Therefore, the  
 156 smoke has been entrained into the ABL over a large area, but the impact  
 157 differs geographically. This was confirmed by Sigler et al. (2003), who re-  
 158 corded high ground-level pollution concentrations on July 7 near Petersham,  
 159 MA (540 km north-east of Baltimore) due to the Canadian forest-fire smoke.  
 160 Note that the visibility at LNS begins to increase again on July 8, after the  
 161 peak period of the haze event, but falls later on. It remains mostly low at  
 162 MTN and BWI (with larger values at BWI) during July 7 and 8, which

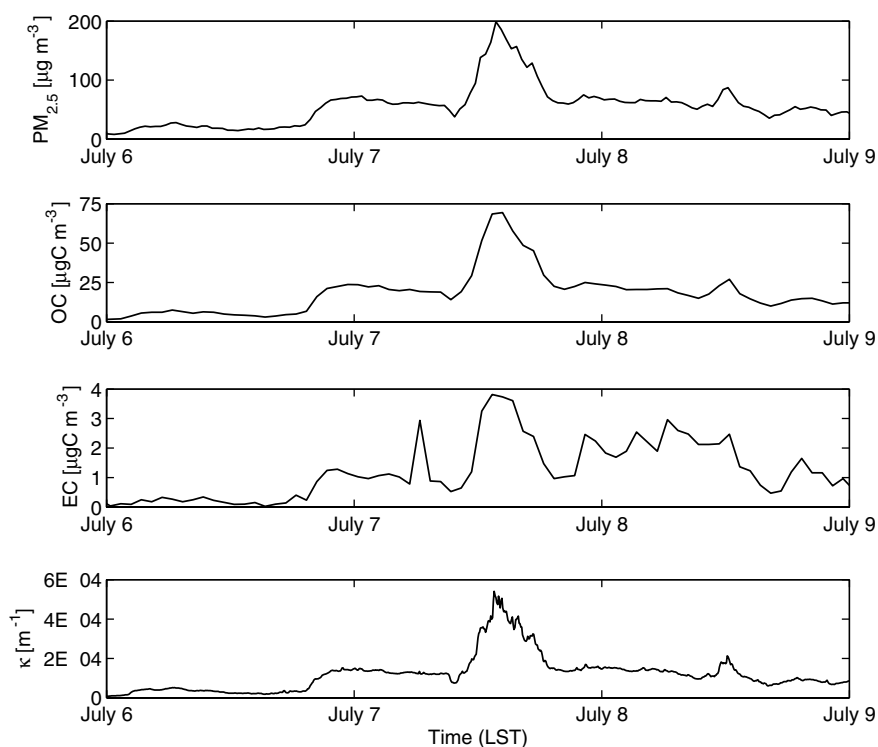


Figure 4. Fine particle ( $<2.5 \mu\text{m}$ ) mass concentration  $\text{PM}_{2.5}$ , organic carbon OC, elemental carbon EC and scattering coefficient  $\kappa$  for the time period July 6–8, 2002. Tick marks along the abscissa axis denote midnight.

163 implies that the aerosols were not removed rapidly and that the atmosphere  
 164 remained turbid.

165 In order to characterise ground-level aerosol during the haze event, the  
 166 fine particle mass concentration  $\text{PM}_{2.5}$ , OC, elemental carbon (EC, effectively  
 167 equivalent to black carbon), and the scattering coefficient  $\kappa$  are shown in  
 168 Figure 4. These four variables are chosen for specific reasons: the  $\text{PM}_{2.5}$   
 169 measurement yields a clear aerosol particle signature, and both OC and EC  
 170 are primary forest-fire combustion products, and therefore serve as a tracer  
 171 for the smoke aerosols caused by the Canadian forest fires. The nephelometer  
 172 data, which yield the scattering coefficient, are related to the lidar measure-  
 173 ments, as both use light scattering as the underlying principle. The effect of  
 174 smoke particles can clearly be seen in the time series of  $\text{PM}_{2.5}$  (Figure 4);  
 175  $\text{PM}_{2.5}$  starts to increase in the evening of July 6 (around 1900 LST), indi-  
 176 cating the arrival of the forest-fire smoke. The maximum  $\text{PM}_{2.5}$  occurs in the  
 177 early afternoon (measurement interval 1315–1345 LST) on July 7 with a  
 178 value of  $198.8 \mu\text{g m}^{-3}$ , and remains elevated after the maximum value (mean

179 concentration on July 8,  $56.0 \mu\text{g m}^{-3}$ ), compared to the concentration before  
 180 the haze event (mean concentration on July 6,  $29.1 \mu\text{g m}^{-3}$ ). The scattering  
 181 coefficient and organic carbon are strongly correlated with  $\text{PM}_{2.5}$ , with  
 182 temporally coinciding maxima ( $\text{OC}_{\text{max}} = 69.4 \mu\text{gC m}^{-3}$ ,  $\kappa_{\text{max}} = 5.41 \times$   
 183  $10^{-4} \text{ m}^{-1}$ ), whereas EC increases at times when  $\text{PM}_{2.5}$  and OC measurements  
 184 remain comparably low. This is due to the fact that EC is only a signature for  
 185 certain forest-fire smoke particles. Depending on the type of fire (e.g. fast  
 186 flaming, smoldering, dry, green, wet) the EC fraction may range from 10% to  
 187 almost zero.

### 5. Lidar Observations of the ABL Structure

189 Time series of boundary-layer height are a good indicator of the strength of  
 190 convective activity in the ABL, because the surface heat fluxes drive the ABL  
 191 diurnally. Figure 5 presents the time series of ABL height for July 6–8, 2002,  
 192 determined from lidar data. The maximum boundary-layer height for July 6  
 193 ( $z_{i,\text{max}} = 1723 \text{ m}$ ) and July 8 ( $z_{i,\text{max}} = 1601 \text{ m}$ ) strongly exceeded the maxi-  
 194 mum ABL height of the peak day of the haze event July 7 ( $z_{i,\text{max}} = 1164 \text{ m}$ ).

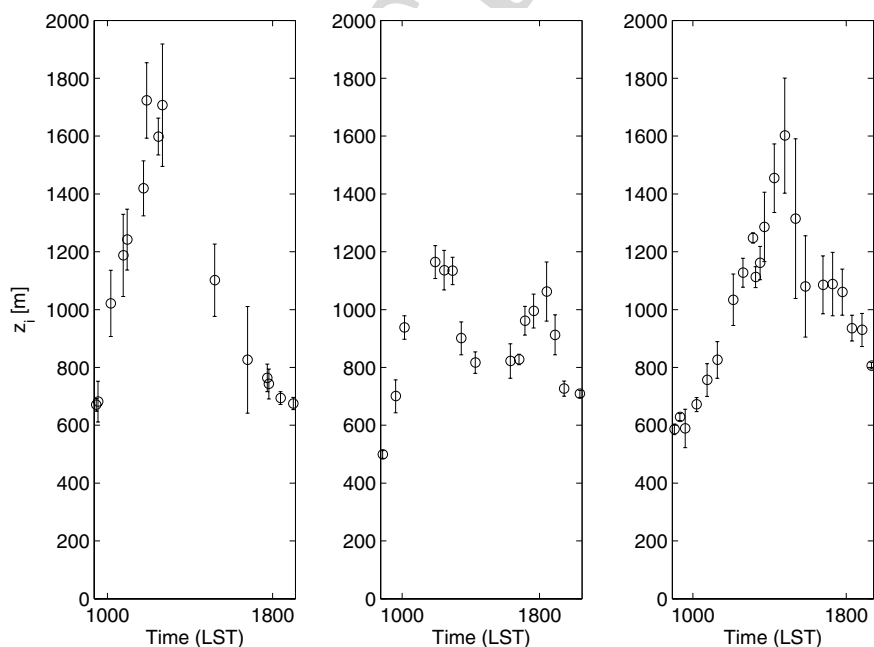


Figure 5. ABL height  $z_i$ , as determined from lidar data using a gradient-contour method, for July 6–8, 2002 (July 6: left panel; July 7: middle panel; July 8: right panel). Error bars denote one standard deviation from the mean for each respective time interval.

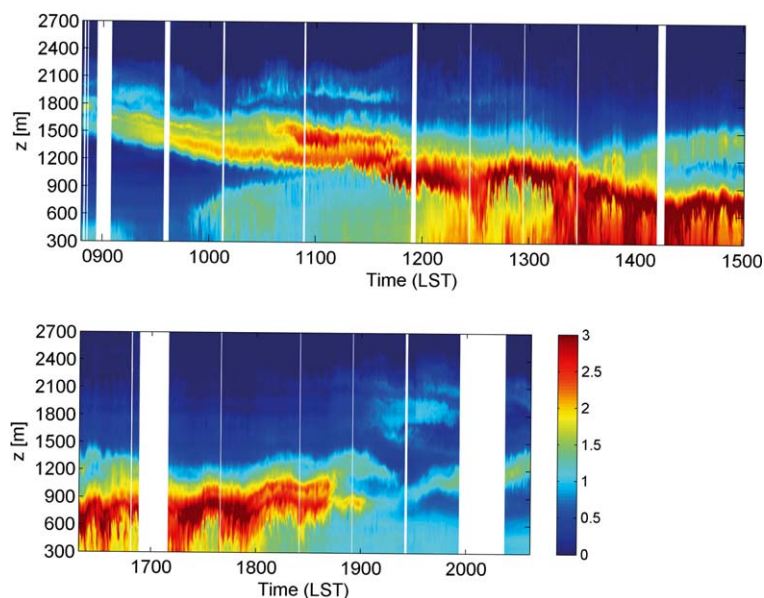


Figure 6. Lidar time series of relative aerosol backscatter from 0847 to 1503 LST (top panel) and from 1618 to 2035 LST (bottom panel).

195 The forest fire smoke reduced solar heating of the ground (see Figure 2d),  
 196 which in turn reduced the surface heat fluxes, thus causing reduced convective  
 197 activity and a lower ABL height.

198 The smoke particles served as flow tracers and provided an excellent vi-  
 199 sualisation of boundary-layer processes. The first lidar backscatter data time  
 200 segment (Figure 6 top panel) from 0847 to 1503 LST shows the coherent  
 201 layer of forest-fire smoke that is forced down to lower altitudes due to  
 202 subsidence over the area. Note the coherence of the smoke plume, ranging  
 203 initially in height from about 1500 to 2250 m. The shallow ( $z_i \approx 500$  m) early  
 204 morning boundary layer is aerosol laden due to rush-hour traffic. Starting at  
 205 around 0950 LST, the growth of the convective boundary layer (CBL) can  
 206 clearly be seen, whereas the smoke layer continues to descend to lower alti-  
 207 tudes (until around 1100 LST). Note that thermals, overshooting at the  
 208 boundary-layer top, create a disturbance in the stably stratified layer aloft,  
 209 which propagates up to the bottom of the smoke layer, manifest in coinciding  
 210 upward and downward movements of air. The dynamic interaction of the  
 211 CBL with the free troposphere has been studied previously (e.g. Gossard and  
 212 Richter, 1970; Metcalf, 1975; Stull, 1976 a, b). Recently, Fochesatto et al.  
 213 (2001), using ground-based lidar, observed dynamic coupling between the  
 214 growing convective boundary layer and the residual layer. They found that  
 215 the top of the residual layer started to fluctuate shortly after the CBL began

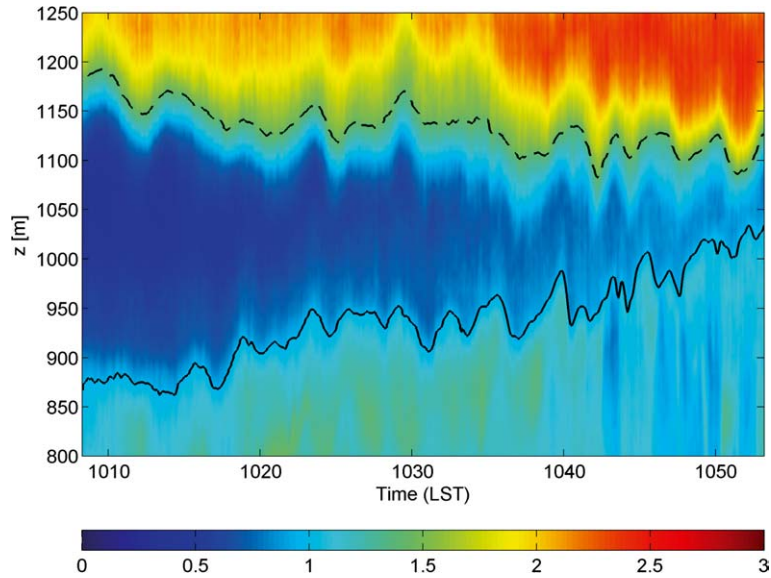


Figure 7. Lidar time series of relative aerosol backscatter from 1008 to 1053 LST. The ABL top and smoke-layer bottom are outlined by the solid and dashed lines, respectively.

216 to develop, indicating gravity waves that were excited by overshooting  
 217 thermals at the top of the CBL.

218 Using smoke as a ‘tracer’, we investigate the interaction between the CBL  
 219 and the overlying air on July 7. In Figure 7 the lidar time series shows the  
 220 growth of the CBL and the descending smoke layer aloft between 1008 and  
 221 1053 LST. From visual inspection, the growing CBL and the overlying  
 222 smoke layer appear to be coupled. Domes forming on top of the CBL  
 223 correspond to the ripple structure at the bottom of the smoke layer. The top  
 224 of the growing convective boundary layer and the bottom of the forest-fire  
 225 smoke layer are determined from the lidar backscatter signal using a com-  
 226 bined gradient-contour method (solid and dashed lines in Figure 7). To  
 227 correlate the two time series we subtract their trends and correlate the  
 228 fluctuations. The correlation coefficient for the time series of fluctuations of  
 229 ABL top and smoke-layer bottom is largest for a time lag of 25 s, with  
 230  $R = 0.48$  (for zero time lag:  $R = 0.37$ ). Since the vertical separation between  
 231 ABL top and smoke-layer bottom ranges from approximately 300 to 60 m,  
 232 the correlation between the two time series is due to wave motion and not  
 233 due to coherent turbulent structures. This maximum correlation for a time  
 234 lag of 25 s is indicative of the group speed of gravity waves excited by  
 235 thermals at the top of the ABL. From the mean distance between ABL top  
 236 and smoke-layer bottom of about 200 m, a mean group speed  $c_g = (200 \text{ m})/$   
 237  $(25 \text{ s}) = 8 \text{ m s}^{-1}$  is determined.

238 Shortly after 1100 LST the smoke layer and the CBL make contact. The  
239 smoke layer atop the CBL serves as a tracer and clearly outlines the thermals  
240 overshooting at the boundary-layer top, and the wisps sinking back into the  
241 CBL. This interplay is known as penetrative convection (Scorer, 1957;  
242 Deardorff et al., 1969; Stull, 1976a). Under regular atmospheric conditions  
243 penetrative convection would result in cleansing of the CBL, since down-  
244 drafts would carry clean free atmospheric air from aloft into the CBL. From  
245 1140 LST onwards the smoke layer is embedded and confined in the  
246 entrainment zone (EZ) due to thermals impinging from the bottom, and due  
247 to the stable free atmosphere (FA) above ('lid effect'). Entrainment charac-  
248 teristics of penetrative convection such as dome (due to thermal updrafts,  
249 Stull, 1976a) and wisp (downdrafts termed 'wisps' by Deardorff et al., 1969)  
250 structures become clearly identifiable throughout the lidar time series. At  
251 around 1230 LST, large amounts of aerosol particles are being 'washed  
252 downward' through the mixed layer to the ground by means of wisps, about  
253 50 min after the smoke layer becomes embedded in the entrainment zone.  
254 Also, from about 1200 LST onward, more aerosols are transported upward  
255 from the surface, since the entrainment of smoke has increased the ground-  
256 level aerosol concentration by that time (see Figure 4). The downward  
257 transport intensifies at around 1315 LST and thereafter. Vigorous downward  
258 mixing in either coherent 'sheets' of aerosols or in broad 'curtains' of aerosols  
259 continues throughout this time period to further degrade air quality within  
260 the mixed layer. Upward and downward transport is almost indiscernible at  
261 this stage. Another process that can be observed is detrainment, the reverse  
262 of entrainment (Deardorff et al., 1980). Small pockets of aerosol-laden air  
263 detrain from the boundary layer, which can be seen clearly at around 1345  
264 LST. This occurs when overshooting thermals do not sink back into the  
265 ABL, but break away and remain in the free atmosphere. Furthermore,  
266 detrainment evolves into a process that will be termed 'detachment'. A  
267 coherent layer of aerosol-laden air separates from the boundary layer at  
268 around 1415 LST, which in turn leads to a decrease of the boundary-layer  
269 height. Relatively clear air separates the CBL from the smoke layer aloft.  
270 This ABL debris might be re-entrained thereafter or remain in the residual  
271 layer or free atmosphere until it becomes re-entrained the following day.  
272 Downward mixing of aerosols continues throughout the afternoon, as can be  
273 seen in the lidar backscatter data time series (Figure 6, bottom panel) from  
274 1618 to 2035 LST. Interestingly, the smoke layer that was confined in the EZ  
275 begins to detach after 1830 LST and the negative impact on air quality  
276 lessens. Along with the decreasing convective activity during the evening  
277 period, penetrative convection ceases. In addition, the inversion at the ABL  
278 top weakens during the transition from daytime, through evening, to  
279 nighttime. Hence the smoke layer, formerly trapped in the entrainment zone,  
280 disconnects and is advected by the large-scale outer flow (see Figure 6,

281 bottom panel). In the process, the layer spreads out and the smoke aerosol  
 282 remains as debris in the residual layer, up to an altitude of about 2400 m.  
 283 However, a coherent layer is lifted off by large-scale motion (near 1930 LST),  
 284 undergoing upward transport and at the same time the stable nocturnal  
 285 boundary layer starts to form.

## 6. Linking ABL and Ground Level Observations

287 Due to the zone of incomplete overlap between the laser beam and the field of  
 288 view of the telescope, a vertically staring lidar can provide information up-  
 289 wards from a certain level only (here  $z_{\min} \approx 300$  m). We investigate the pos-  
 290 sible link between ABL entrainment and mixing, as observed with the lidar,  
 291 to *in situ* ground-level measurements. Of particular importance is the com-  
 292 parison between remotely sensed lidar data in the mixed layer and data  
 293 obtained from *in situ* measurements in the atmospheric surface layer. Since  
 294 the time series of the scattering coefficient on July 7 is representative of the  
 295 temporal evolution of  $\text{PM}_{2.5}$ , OC, and also of EC during the peak period (see  
 296 Figure 4), and since  $\kappa$  is available at higher temporal resolution, we use the  
 297 nephelometer data to compare with relative aerosol backscatter data from  
 298 the lidar. The lidar and nephelometer serve as a means a to determine the  
 299 upward (through thermals) and downward (through wisps) transport of  
 300 aerosols through the surface layer and mixed layer. Concentrations in both  
 301 time series are related to the occurrence of these events. Mixing due to tur-  
 302 bulence of smaller scales also contributes to a vertical homogenization of the  
 303 flow, but the mixing due to large scales is dominant in convective conditions.  
 304 Thorough mixing of smoke aerosols in the whole ABL will increase the lidar  
 305 backscatter signal throughout, as well as the scattering coefficient of the  
 306 nephelometer on the ground. Plots of lidar transects (5-min moving average)  
 307 at several heights, along with the nephelometer data, are presented in Fig-  
 308 ure 8. For ready comparison, the vertical axis is normalised by the respective  
 309 maximum value of each measurement. The nephelometer data and lidar data  
 310 at a certain level correspond well for distinct, yet certainly not all, time  
 311 periods. The lidar signal at  $z = 1246$  m always samples the free atmosphere,  
 312 since the maximum ABL height is 1164 m. In the morning the lidar signal at  
 313  $z = 1246$  m samples the smoke layer descent above the ABL and hence is  
 314 larger than the nephelometer data. In the afternoon the smoke layer is  
 315 embedded in the ABL such that the lidar at  $z = 1246$  m samples free  
 316 atmospheric air with smaller smoke concentrations than at the ground. When  
 317 levels within the ABL are chosen, the correlations are larger and increase  
 318 with proximity to the ground. The increase in correlation can clearly be seen  
 319 from Figure 8 for a few selected representative levels. The intermediate  
 320 height,  $z = 875$  m, alternately lies above and below  $z_i$ , corresponding to

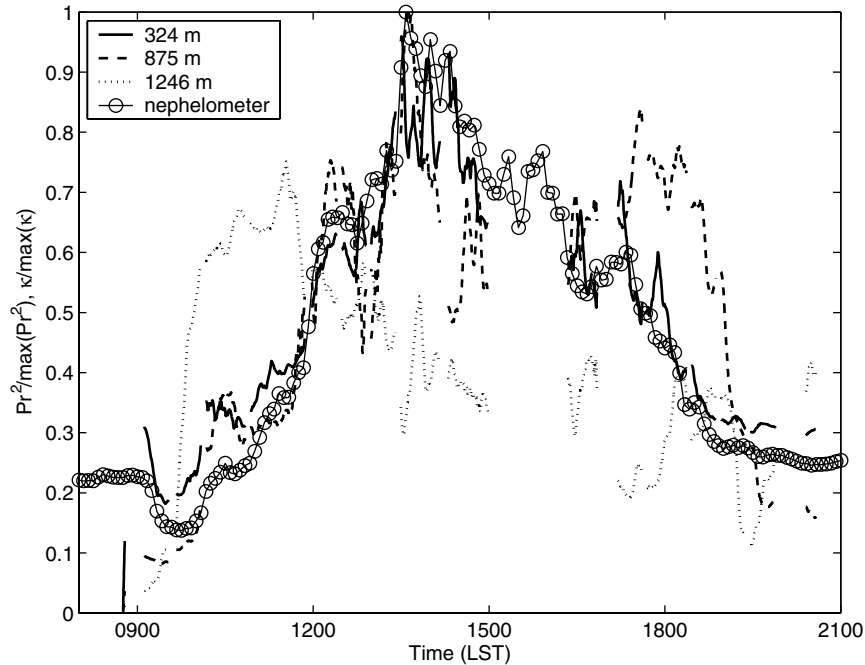


Figure 8. Lidar transects (5-min moving average) at different heights and nephelometer data for July 7, 2002. The lidar (lidar data  $P$  corrected with  $r^2$ , where  $r$  is range from the lidar) and nephelometer data are normalised by their respective maximum values. The levels were chosen to lie always below  $z_i$  (level  $z = 324$  m), alternating above and below  $z_i$  (level  $z = 875$  m) and always above  $z_i$  (level  $z = 1246$  m).

321 varying agreement with the nephelometer. Between 1800 and 1900 LST the  
 322 smoke layer lifts, hence the aerosol concentration increases in this height  
 323 region, and therefore the lower correlation with ground-level observations.  
 324 The height  $z = 324$  m lies always within the ABL during the time period  
 325 under consideration and exhibits a strong correlation between lidar and  
 326 nephelometer ( $R = 0.96$ ). The data correlate best for zero time lag. Table I  
 327 summarises the comparison between lidar and nephelometer in the form of a  
 328 correlation matrix. The high correlation coefficient  $R$  between the lidar at  
 329 324 m and nephelometer suggests strong coupling of the lower mixed layer  
 330 and near surface air pollution levels for time scales  $>5$  min. Measurements at  
 331 levels that were always below  $z_i$  ( $z = 324$  and 504 m) show the highest cor-  
 332 relation with each other and with ground-level observations.

333 Two interesting events, as observed with lidar, were corroborated by  
 334 nephelometer data. From 0915 to 0950 LST a strong decrease in the lidar  
 335 signal was recorded at low altitudes (see Figure 6, top panel). This corre-  
 336 sponds to a strong decrease in the scattering coefficient measured at the  
 337 ground (see Figure 8). A possible cause is the reduction of ambient aerosol

TABLE I

Matrix of correlation coefficient  $R$  for lidar transects at several levels (normalised relative aerosol backscatter) and nephelometer 'neph' (normalised scattering coefficient, measured at ground level).

	324 m	504 m	684 m	875 m	1066 m	1246 m	neph
324 m	1.00	0.94	0.82	0.72	0.51	0.12	0.96
504 m	0.94	1.00	0.88	0.72	0.44	0.09	0.89
684 m	0.82	0.88	1.00	0.74	0.35	0.004	0.81
875 m	0.72	0.72	0.74	1.00	0.63	0.08	0.75
1066 m	0.51	0.44	0.35	0.63	1.00	0.39	0.56
1246 m	0.12	0.09	0.004	0.08	0.39	1.00	0.12
Neph	0.96	0.89	0.81	0.75	0.56	0.12	1.00

Levels  $z = 324$  and  $504$  m were always below  $z_i$ ,  $z = 684, 875$  and  $1066$  m were alternating above and below  $z_i$  and  $z = 1246$  m was always above  $z_i$ .

338 from car exhaust after the morning rush-hour traffic. Secondly, the detach-  
 339 ment of a coherent smoke layer from the ABL, starting at about 1400 LST  
 340 (see Figure 6, top panel) corresponds to the onset of the decrease in the  
 341 scattering coefficient in the early afternoon, as obtained from the nephe-  
 342 lometer. Hence, this removal of aerosol through the top of the ABL affected  
 343 the aerosol concentration throughout the boundary layer.

## 7. Discussion

345 It has been shown how forest-fire smoke can, under particular, yet not  
 346 unusual, synoptic atmospheric conditions, substantially affect air quality and  
 347 regional climate in regions remote from the fire origin. In the Québec forest-  
 348 fire event of July 7, 2002, in Baltimore, the interplay of smoke that is ad-  
 349 vected by synoptic winds, large-scale subsidence and boundary-layer  
 350 entrainment is responsible for high particle concentrations throughout the  
 351 ABL, down to the ground. The smoke event presented a unique opportunity  
 352 to study ABL characteristics using lidar.

353 Reflection and absorption of sunlight by a dense elevated smoke layer  
 354 acted to lower daytime air temperature and possibly strengthen the ABL  
 355 inversion. This contrasts with the regular case, where direct heating by  
 356 shortwave radiation absorbed by aerosols *within* the boundary layer is found  
 357 to be an important component of the boundary-layer heat budget (Angevine  
 358 et al., 1998b). However, if larger amounts of aerosol are present in the  
 359 atmosphere, the opposite can occur, as was shown here and elsewhere  
 360 (Robock, 1988a, b; Menon et al., 2002), with implications for regional scale  
 361 climate.

362 A prime purpose of our study was to investigate the structure of the  
363 atmospheric boundary layer in great detail, using the smoke particles as  
364 tracers. Several mechanisms were observed, such as dry convection, mixing  
365 inside the ABL, entrainment, and detrainment. We would like to note that  
366 detrainment, as observed in our study, differs greatly from detrainment ob-  
367 served for slope flows under stable atmospheric conditions (Monti et al.,  
368 2002), or in laboratory experiments (Fernando et al., 2001). In those cases,  
369 fluid can peel off as it flows upslope or downslope. As was shown by the lidar  
370 data time series taken during the haze event, pockets of boundary-layer air  
371 can overshoot the top of the ABL and break away under convective condi-  
372 tions.

373 Internal gravity waves can be excited in the non-turbulent region above  
374 the ABL by penetrative convection (Stull, 1976b). Our analysis (see Figure 7)  
375 confirms that disturbances, caused by overshooting thermals, can propagate  
376 vertically upward, away from the ABL.

377 There are some similarities between a cloud-topped boundary layer and  
378 the ABL on July 7, 2002, which was initially topped by a smoke layer. A  
379 smoke-topped ABL shares with the stratocumulus-topped ABL the essential  
380 features of turbulence and entrainment driven by radiative cooling (Moeng  
381 et al., 1999). The forest-fire smoke layer caused strong absorption of solar  
382 shortwave radiation due to black carbon ('soot'), which is re-emitted as  
383 longwave radiation, leading to radiative cooling. Shortwave radiation can  
384 also be simply reflected back to space (e.g. by non-absorbing particles such as  
385 organic carbon). In a large-eddy simulation study of the ABL driven by  
386 smoke-cloud-top radiative cooling only (hence not fully comparable to the  
387 convectively driven ABL here) by Moeng et al. (1999), it was found that the  
388 entrainment rate depends substantially on the jump in longwave radiative  
389 flux above the entrainment buoyancy flux level. Furthermore, the radiative  
390 flux divergence was found to exist solely within the smoke region, which cools  
391 the smoke-cloud layer and thus enhances the local inversion strength.  
392 Noteworthy, there is the study by Robock (1988b) who found that forest-fire  
393 smoke trapped in a valley strengthened the inversion by preventing surface  
394 warming due to solar radiation, there by enhancing the smoke trapping and  
395 surface cooling in a positive feedback loop. These studies explain, in part, the  
396 strong lid effect of the smoke layer found here. In addition, they provide a  
397 physical explanation for the tremendously energetic wisps that carry large  
398 amounts of aerosol downward. These wisps originate within the entrainment  
399 zone, perhaps cooled due to radiative effects, and hence the EZ air mass  
400 becomes negatively buoyant, promoting energetic downward transport.  
401 Furthermore, note that the process of detachment might have been caused in  
402 part by differential absorption of sunlight. In an analogy to studies on the  
403 stratocumulus-topped ABL (e.g. Slingo et al., 1982; Driedonks and  
404 Duijnkerke, 1989; Moeng, 1998) it appears that shortwave radiative heating



405 (positive buoyant forcing) and longwave cooling (negative buoyant forcing)  
406 destabilises the smoke layer and leads to detachment.

407 The smoke layer was initially above the ABL and intersected with the  
408 growing ABL due to subsidence. Since the process can be viewed as a type of  
409 fumigation, it is reasonable to compare the results with the study by Dear-  
410 dorff and Willis (1982). They found that the ground-level concentration was  
411 maximised 1–2 h after the fumigation process began. In the current study the  
412 start of fumigation is around 1140 LST, and the maximum scattering coef-  
413 ficient from the nephelometer was measured during the sampling interval  
414 1330–1335 LST. Thus, a time lag of about 2 h is observed, which compares  
415 well with the result of Deardorff and Willis. Furthermore, the lidar visuali-  
416 sations show that wisps do not initially reach the ground; hence the fumigant  
417 is intercepted spottily by the mixed layer, producing the time lag, in agree-  
418 ment with Deardorff and Willis.

### Acknowledgements

420 The authors wish to thank Mariana Adam, Chad Higgins, Elie Bou-Zeid and  
421 Vijayant Kumar (Johns Hopkins University) for their assistance in the field.  
422 We gratefully acknowledge the loan of equipment by Prof. Phil Hopke  
423 (Clarkson University). We would also like to thank the MODIS Land Rapid  
424 Response Team (NASA/GSFC, Greenbelt, Maryland) for permission to use  
425 MODIS images. This research has been supported by the U.S. Environ-  
426 mental Protection Agency (EPA 99-NCERQA-X1).

### References

- 428 Albertson, J. D. and Parlange, M. B.: 1999, 'Surface Length Scales and Shear Stress: Impli-  
429 cations for Land-Atmosphere Interaction over Complex Terrain', *Water Resour. Res.* **35**,  
430 2121–2132.
- 431 Angevine, W. M., Grimsdell, A. W., Hartten, L. M., and Delany, A. C.: 1998a, 'The Flatland  
432 Boundary Layer Experiment', *Bull. Amer. Meteorol. Soc.*, **79**, 419–431.
- 433 Angevine, W. M., Grimsdell, A. W., McKeen, S. A., and Warnock, J. M.: 1998b, 'Entrain-  
434 ment Results from the Flatland Boundary Layer Experiments', *J. Geophys. Res.* **103**,  
435 13689–13701.
- 436 Deardorff, J. W., Willis, G. E., and Lilly, D. K.: 1969, 'Laboratory Investigation of Nonsteady  
437 Penetrative Convection', *J. Fluid Mech.* **35**, 7–31.
- 438 Deardorff, J. W., Willis, G. E., and Stockton, B. H.: 1980, 'Laboratory Studies of the  
439 Entrainment Zone of a Convectively Mixed Layer', *J. Fluid Mech.* **100**, 41–64.
- 440 Deardorff, J. W. and Willis, G. E.: 1982, 'Ground-level Concentrations Due to Fumigation  
441 into an Entraining Mixed Layer', *Atmos. Environ.* **16**, 1159–1170.
- 442 Driedonks, A. G. M. and Duynkerke, P. G.: 1989, 'Current Problems in the Stratocumulus-  
443 topped Atmospheric Boundary Layer', *Boundary-Layer Meteorol.* **46**, 275–303.

- 444 Fedorovich, E. and Thäter, J.: 2002, 'A Wind Tunnel Study of Gaseous Tracer Dispersion in  
445 the Convective Boundary Layer Capped by a Temperature Inversion', *Atmos. Environ.* **36**,  
446 2245–2255.
- 447 Fernando, H. J. S., Lee, S. M., Anderson, J., Princevac, M., Pardyjak, E., and Grossmann-  
448 Clarke, S.: 2001, 'Urban Fluid Mechanics: Air circulation and Contaminant Dispersion in  
449 Cities', *Environ. Fluid Mech.* **1**, 107–164.
- 450 Fochesatto, G. J., Drobinski, P., Flamant, C., Guedalia, D., Sarrat, C., Flamant, P. H., and  
451 Pelon, J.: 2001, 'Evidence of Dynamic Coupling Between the Residual Layer and the  
452 Developing Convective Boundary Layer', *Boundary-Layer Meteorol.* **99**, 451–464.
- 453 Forster, C., Wandinger, U., Wotawa, G., James, P., Mattis, I., Althausen, D., Simmonds, P.,  
454 O'Doherty, S., Jennings, S. G., Kleefeld, C., Schneider, J., Trickl T., Kreipl, S., Jager, H.,  
455 and Stohl A.: 2001, 'Transport of Boreal Forest Fire Emissions from Canada to Europe',  
456 *J. Geophys. Res.* **106**, 22887–22906.
- 457 Garratt, J. R.: 1992, *The Atmospheric Boundary Layer*, Cambridge University Press, Cam-  
458 bridge, U.K. 316 pp.
- 459 Gossard, E. and Richter, J. H.: 1970, 'The Shape of Internal Waves of Finite Amplitude from  
460 High Resolution Radar Sounding of the Lower Atmosphere', *J. Atmos. Sci.* **27**, 971–973.
- 461 Iziomon, M. G. and Lohmann, U.: 2003, 'Optical and Meteorological Properties of Smoke-  
462 dominated Haze at the ARM Southern Great Plains Central Facility', *Geophys. Res. Lett.*  
463 **30**, doi:10.1029/2002GL016606.
- 464 Menon, S., Hansen, J., Nazarenko, L., and Luo, Y.: 2002, 'Climate Effects of Black Carbon  
465 Aerosols in China and India', *Science* **297**, 2250–2253.
- 466 Menut, L., Flamant, C., Pelon, J., and Flamant, P. H.: 1999, 'Urban Boundary-layer Height  
467 determination from Lidar Measurements over the Paris Area', *Appl. Opt.* **38**, 945–954.
- 468 Metcalf, J. I.: 1975, 'Gravity Waves in a Low Level Inversion', *J. Atmos. Sci.* **32**, 351–361.
- 469 Moeng, C.-H.: 1998, 'Stratocumulus-topped Atmospheric Planetary Boundary Layer', in E. J.  
470 Plate et al. (eds.), *Buoyant Convection in Geophysical Flows*, NATO Science Series C, vol.  
471 513, Kluwer Academic Publishers, Dordrecht, pp. 421–440.
- 472 Moeng, C.-H., Sullivan, P. P., and Stevens, B.: 1999, 'Including Radiative Effects in an  
473 Entrainment Rate Formula for Buoyancy-Driven PBLs', *J. Atmos. Sci.* **56**, 1031–1049.
- 474 Monti, P., Fernando, H. J. S., Princevac, M., Chan, W. C., Kowalewski, T. A., and Pardyjak,  
475 E. R.: 2002, 'Observations of Flow and Turbulence in the Nocturnal Boundary Layer over  
476 a Slope', *J. Atmos. Sci.* **59**, 2513–2534.
- 477 Pahlow, M.: 2002, *Atmospheric Boundary Layer Dynamics and Inversion Technologies to Ob-  
478 tain Extinction Coefficient Profiles in the Atmosphere from Elastic Lidar*, Ph.D. Disserta-  
479 tion, Johns Hopkins University, Baltimore, MD, USA, 209 pp.
- 480 Robock, A.: 1988a, 'Enhancement of Surface Cooling due to Forest Fire Smoke', *Science* **242**,  
481 911–913.
- 482 Robock, A.: 1988b, 'Surface Temperature Effects of Forest Fire Smoke Plumes', in P. V.  
483 Hobbs and M. P. McCormick (eds.), *Aerosols and Climate*, Deepak Publishing, Hampton,  
484 VA, pp. 435–442.
- 485 Scorer, R. S.: 1957, 'Experiment on Convection of Isolated Masses of Buoyant Fluid', *J. Fluid  
486 Mech.* **2**, 583–594.
- 487 Sigler, J. M., Lee, X., and Munger, W.: 2003, 'Emission and Long-range Transport of Gaseous  
488 Mercury from a Large-scale Canadian Boreal Forest Fire', *Environ. Sci. Technol.* **37**, 4343–  
489 4347.
- 490 Skinner, W. R., Stocks, B. J., Martell, D. L., Bonsal, B., and Shabbar, A.: 1999, 'The  
491 Association Between Circulation Anomalies in the Mid-troposphere and Area Burned by  
492 Wildland Fire in Canada', *Theor. Appl. Climatol.* **63**, 89–105.

- 493 Skinner, W. R., Flannigan, M. D., Stocks, B. J., Martell, D. L., Wotton, B. M., Todd, J. B.,  
 494 Mason, J. A., Logan, K. A., and Bosch, E. M.: 2002, 'A 500 hPa Synoptic Wildland Fire  
 495 Climatology for Large Canadian Forest Fires, 1959–1996', *Theor. Appl. Climatol.* **71**, 157–  
 496 169.
- 497 Slingo, A., Nicholls, S., and Schmertz, J.: 1982, 'Aircraft Observations of Marine Stratocu-  
 498 mulus During JASIN', *Quart. J. Roy. Meteorol. Soc.* **108**, 833–856.
- 499 Stull, R. B.: 1976a, 'The Energetics of Entrainment Across a Density Interface', *J. Atmos. Sci.*  
 500 **33**, 1260–1267.
- 501 Stull, R. B.: 1976b, 'Internal Gravity Waves Generated by Penetrative Convection', *J. Atmos.*  
 502 *Sci.* **33**, 1279–1286.
- 503 Stull, R. B.: 1988, *An Introduction to Boundary Layer Meteorology*, Kluwer Academic Pub-  
 504 lishers, Dordrecht, 666 pp.
- 505 Sullivan, P. P., Moeng, C.-H., Stevens, B., Lenshow, D. H., and Mayor, S. D.: 1998,  
 506 'Structure of the Entrainment Zone Capping the Convective Atmospheric Boundary  
 507 Layer', *J. Atmos. Sci.* **55**, 3042–3064.
- 508 Weber, M. G. and Stocks, B. J.: 1998, 'Forest Fires and Sustainability in the Boreal Forests of  
 509 Canada', *Ambio.* **27**, 545–550.
- 510 Wotawa, G. and Trainer, M.: 2000, 'The Influence of Canadian forest Fires on Pollutant  
 511 Concentrations in the United States'. *Science.* **288**, 324–328.
- 512 Wyngaard, J. C. and Brost, R. A.: 1984, 'Top-down and bottom-up diffusion of a Scalar in the  
 513 Convective Boundary Layer', *J. Atmos. Sci.* **41**, 102–112.
- 514 Yi, C., Davis, K. J., Berger, B. W., and Bakwin, P. S.: 2001, 'Long-term Observations of the  
 515 Dynamics of the Continental Planetary Boundary Layer', *J. Atmos. Sci.* **58**, 1288–1299.  
 516